Agglomerates and Aggregates: Number and Size of Primary Particles from *in-situ* Mass-Mobility Measurements

M.L. Eggersdorfer[1], A.J. Groehn[1], C.M. Sorensen[2], P.H. McMurry[3] and S.E. Pratsinis[1*]

[1]Swiss Federal Institute of Technology, ETH Zurich,
Sonneggstrasse 3, CH-8092 Zürich, Switzerland
[2]Kansas State University, Manhattan, KS, USA
[3]University of Minnesota, Minneapolis, MN, USA
*corresponding author: pratsinis@ptl.mavt.ethz.ch

ABSTRACT

Rapid characterization of gas-borne nanoparticles is important for monitoring aerosol synthesis as well as environmental particle concentrations. Here, the formation of aggregates by viscous flow sintering of amorphous materials (silica, polymers) and grain boundary diffusion sintering of crystalline ceramics (titania, alumina) or metals (Ni, Fe, Ag etc.) is investigated by multiparticle sintering simulations. A scaling law is discovered between average aggregate projected area and equivalent number of constituent primary particles during sintering. This is a relation essentially independent of time, material properties and sintering mechanisms. So the surface area mean primary particle diameter is determined by (on-line) differential mobility analyzer (DMA) and aerosol particle mass (APM) analyzer measurements and this power law for aggregates. This is in good agreement with the primary particle diameter obtained by nitrogen adsorption.

Keywords: differential mobility analyzer, aerosol particle mass measurement, specific surface area, particle diameter.

1 INTRODUCTION

Gas-borne nanoparticles generated at high temperatures undergo coagulation forming agglomerates (physically-bound particles) and aggregates (chemically- or sinter-bound particles). The structure of such particles influences their transport, light scattering, effective surface area and density. Real-time characterization of nanoparticles is necessary for continuous monitoring of aerosol manufacturing and airborne pollutant particle concentrations, but is still challenging [1]. Mostly ex-situ methods have been used to characterize such structures in terms of agglomerate mass, mobility and radius of gyration, mass fractal dimension, D_f, primary particle diameter and number and specific surface area (SSA). Figure 1 shows a sphere, an aggregate [2] and agglomerate [3] having the same mobility diameter, d_m, but different mass, m, and surface area, a. The mobility diameter in the free molecular and transition regime is determined with the average projected area [4]. So measuring only one particle property is not sufficient to characterize those structures.

Here, zirconia nanoparticles are generated by a scalable flame spray process and are characterized in almost real-time with their mass and mobility diameter. The mobility diameter is measured by a differential mobility analyser (DMA) and the mass by an aerosol particle mass analyser (APM) to determine the mass-mobility exponent (D_{fm}). Additionally, multiparticle sintering simulations are performed resulting in a new relation [5] between average primary particle diameter, aggregate/agglomerate mass and mobility diameter. This relation is used to extract the primary particle diameter or SSA from these DMA-APM data. The effect of oxygen flow and precursor feed rate as well as precursor concentration on agglomerate/aggregate structure and primary particle diameter are investigated. Good agreement between ex-situ nitrogen adsorption (BET) and on-line DMA-APM is found for all investigated process conditions.

2 THEORY

2.1 Mulitparticle Sintering Dynamics

Agglomerates containing 16-512 primary particles are generated by diffusion-limited cluster-cluster agglomeration [DLCA, 6] and are sintered by viscous flow [2] and grain boundary diffusion [5]. The driving force for sintering is the minimization of free energy. For amorphous materials (e.g. silica, polymers), this energy minimization results in a viscous flow and reduction of surface area. In crystalline materials (e.g. titania, alumina, Ag, Ni) a grain boundary forms between misaligned crystals. The stress gradient between neck surface and grain boundary causes a flux of atoms into the neck and also a reduction of surface area as has been shown recently by molecular dynamics simulations [7]. The particle centers approach each other and both mechanisms end in full coalescence. The change in particle distance dx/dt and particle growth rate dr/dt are calculated by energy and mass balances [2]. This allows simulating the restructuring of the whole aggregate and to monitor its properties during sintering.

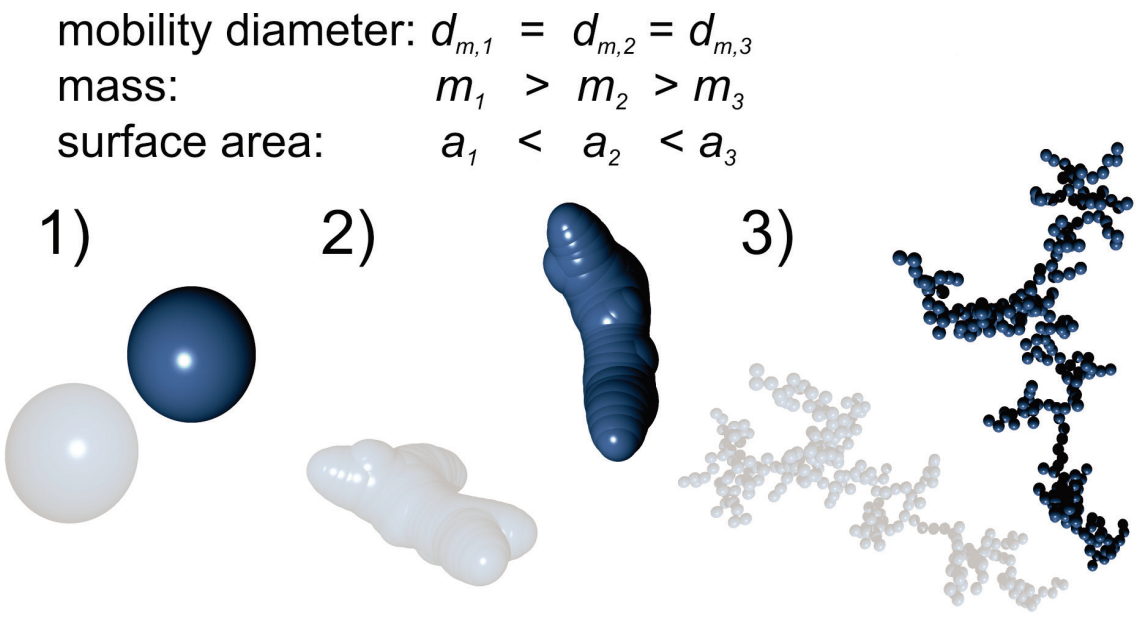

Figure 1: Snapshots of simulated nanoparticle structures: 1) Sphere, 2) aggregate & 3) agglomerate. All have the same mobility diameter, d_m, but different mass, m, and surface area, a. Measuring two of these properties allows the determination of the third one [5].

2.2 Agglomerate/Aggregate Mobility & Primary Particle Diameter

The mobility diameter, d_m, of an agglomerate or aggregate in the free molecular and partly transition regime corresponds to its rotationally averaged projected area, a_a [4]:

$$d_m = \sqrt{\frac{4a_a}{\pi}} \tag{1}$$

The equivalent primary particle diameter, d_{va}, of an agglomerate/aggregate as a function of d_m and m is [5]:

$$d_{va} = \frac{6m}{a\rho} = \left(\frac{\pi k_a \rho}{6m} \left(d_m\right)^{2D_a} \right)^{1/(2D_a-3)} \tag{2}$$

where ρ is the particle density and D_a = 1.07 and k_a = 1.0 are constants obtained from the sintering simulations [5].

3 EXPERIMENTAL

Figure 1 shows a sketch of the experimental setup. Fractal-like zirconia (ZrO_2) particles were generated by oxidation of Valirex Zr 18% Ester with Zirconium 2-ethylhexanoic acid (ZrEHA, Umicore) precursor in a flame spray pyrolysis (FSP) unit [8]. The precursor, X, and oxygen, Y, flow rates are used to characterize the flame as X/Y flame, e.g. a flame with 4 ml/min precursor and 5 l/min O_2 flow rate is called 4/5 flame. The flame-made ZrO_2 was sampled by a probe along the flame centerline at 15 – 30 cm height above burner (HAB) at radially well mixed conditions. The sample aerosol was diluted twice, first by a factor of 10 in a water cooled, custom-made diluter with particle-free air and then in a rotating disk diluter (MD19-1E, Matter Engineering AG) with a variable dilution factor of about 20 – 200. So the number concentration is reduced down to approximately 10^6 to 10^7 cm^{-3}. A soft x-ray neutralizer (Model 3087, TSI Inc.) brought the particles to a Boltzmann equilibrium charge distribution before they were size-classified by a differential mobility analyzer (DMA, Model 3081, TSI Inc.). The sheath and aerosol sample flow rates in the DMA were 4 - 7 and 1.5 l/min, respectively. The agglomerate or aggregate mass, m, was obtained with an aerosol particle mass (APM, Model APM-3600, Kanomax) analyzer using the mode of the APM mass distribution as the average m [9]. A condensation particle counter (CPC, Model 3775, TSI Inc.) measured the number concentration after the APM. Polystyrene latex spheres (d_p = 100 - 300 nm, PSL, Duke Scientific Corporation) were used to validate the DMA-APM system. The measured m and d_m relation by a DMA-APM is:

$$m = k_{APM} \left(d_m\right)^{D_{fm}} \tag{3}$$

where k_{APM} is a constant prefactor and D_{fm} the mass-mobility exponent [9].

Particles were also collected on a glass-fiber filter to determine the product powder specific surface area (*SSA*) from a five-point nitrogen adsorption isotherm at 77.3 K (Micromeritics Tristar 3000). The samples were degassed in nitrogen at 150 °C for at least one hour (Micromeritics Flow prep 060) before adsorption to remove water bound to

the surface from air moisture. The BET-equivalent primary particle diameter is calculated as $d_{BET} = d_{va} = 6/(\rho \cdot SSA)$.

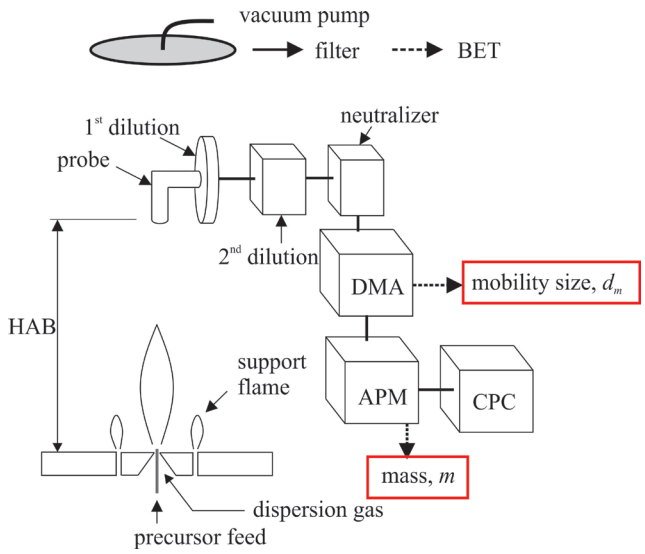

Figure 2: Schematic of experimental setup: The aerosol is sampled at a certain HAB (height above burner), diluted twice and size selected in a DMA (differential mobility analyzer) and mass segregated in an APM (aerosol particle mass analyzer). Finally the concentration is measured with a CPC (condensation particle counter).

4 RESULTS & DISCUSSION

4.1 Sintering Dynamics

First, the two-particle sintering model is validated with simulations [10] and experiments [2]. Figure 3 shows the evolution of the neck radius for different particle size ratios, R_0/r_0, as a funciton of dimensionless time, $t\gamma/(\eta r_0)$, where γ is the surface energy, η the viscosity and r_0 the initial primary particle radius. At the beginning, the difference in curvatures in the neck region and therefore the pressure towards a reduction of the surface area are highest. A 15% faster neck radius growth of the present work than that by Kirchhof et al. [10, symbols] is found due to the simplifying assumptions of the present model described in detail in [2]. Nevertheless the same trend is found as larger particle size ratios lead to faster sinter neck growth. The high flexibility to simulate large systems and the relative accuracy of the proposed model justifies the usage of the present simplifications. A larger difference in size ratio leads to a faster increase in the neck radius as the difference in curvatures is larger, which is the driving force for sintering. Yet it takes longer until full coalescence is reached if the time is normalized by the initial size of the small particle. The smaller particle's curvature needs to adjust to the curvature of the fully coalesced sphere, which takes longer with increasing particle size difference.

Medalia et al. [11] found that a power scaling between primary particle number, n_p, and a_a exists for agglomerates of monodisperse spherical primary particles in point contact. The multiparticle sintering simulations [2,5] show that this power law holds also during sintering nearly independent of sintering mechanism, time or material. Thus this power law (utilized for eq. 2) is used to characterize ZrO_2 nanoparticle agglomerates and aggregates by mass-mobility measurements in the next section.

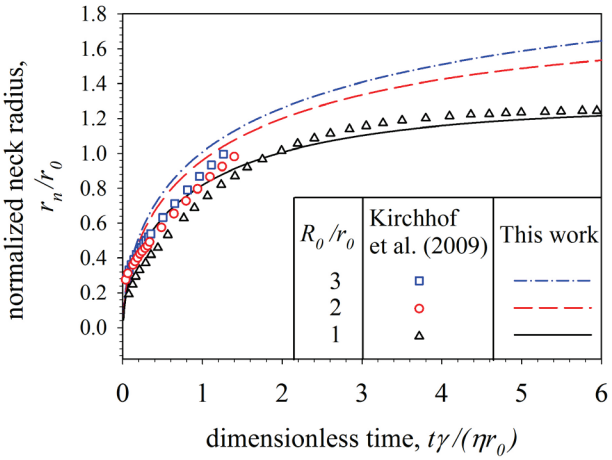

Figure 3: The evolution of the neck radius with dimensionless time for differently sized pairs of particles is compared to simulations of Kirchhof et al. [10].

4.2 Mass-mobility Measurements

Figure 4 shows the effect of O_2 flow rate on D_{fm} and k_{APM} for 4 l/min ZrEHA precursor feed rate. The D_{fm} is fitted to the measured d_m and m in a double logarithmic plot and corresponds to the slope of the dashed hairline through each set of data points. The prefactor k_{APM} equals the value on the line at $d_m = 1$. The agglomerates have a $D_{fm} \approx 2.15$ consistent with cluster-cluster agglomerates [12] or aggregates at the beginning of sintering [5] independent of O_2 flow rate. Cluster-cluster agglomerates with $D_{fm} = 2.1 - 2.2$ are typically open, chain-like structures with a $D_f \approx 1.8$-1.9 and are formed by clusters following either ballistic or diffusion-limited trajectories [3]. The ZrO_2 agglomerate mass at a measured d_m decreases with increasing O_2 flow rate, which is an indication of smaller primary particles.

Higher O_2 flow rates result in a shorter flame, higher flow velocity, additional ambient air entrainment, higher flame cooling rate and thus a shorter particle residence time at high temperature as well as lower ZrO_2 concentration reducing coagulation and d_{va} [8]. So the d_{va} decreases from 14.7 nm at 3 lpm to 9.7 nm at 7 lpm O_2 flow rate (Fig. 5) from BET measurements. Most notably, Fig. 5 shows also the d_{va} from *in-situ* DMA-APM analysis using eq. 2 (squares). The d_{va} by DMA-APM is in good agreement with BET measurements for all O_2 flow rates, which supports the model assumption that the mobility diameter is proportional to the projected agglomerate area.

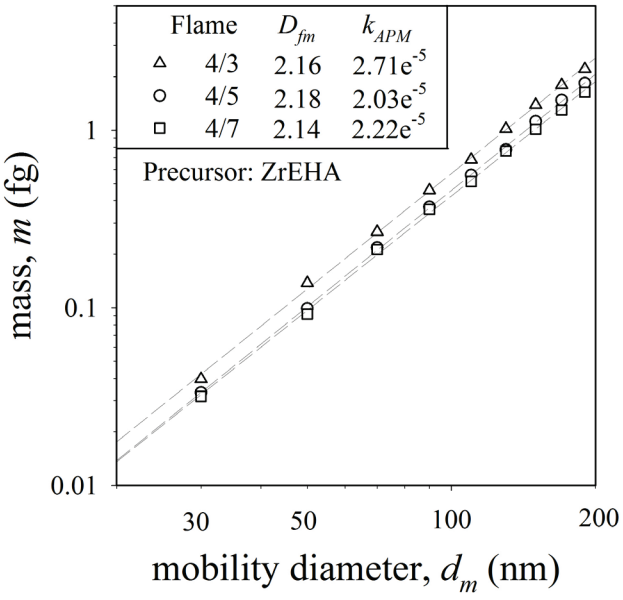

Figure 4: The effect of O_2 flow rate on mass-mobility exponent, D_{fm}, prefactor, k_{APM}, is investigated for 4 ml/min precursor flow rate at 0.5 mol/l Zr concentration. The D_{fm} are independent of the O_2 flow rate varying from 3 – 7 l/min and are consistent with D_{fm} for cluster-cluster agglomerates [12] or aggregates at the beginning of sintering [5].

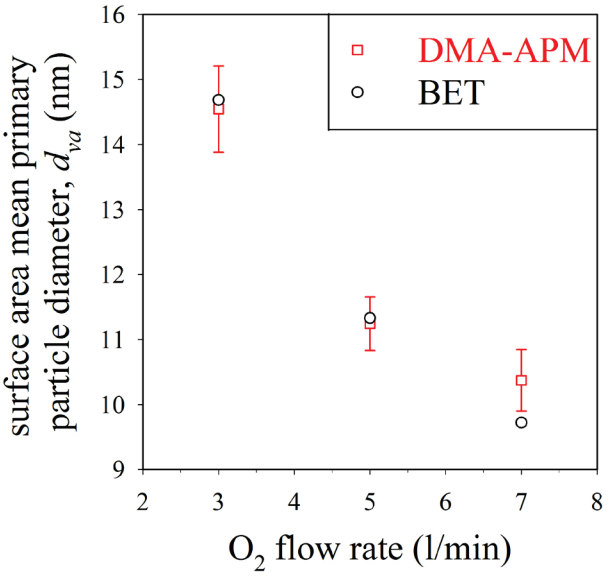

Figure 5: Effect of oxygen flow rate on the average primary particle diameter (inverse of SSA) measured by ex-situ BET and on-line DMA-APM measurements using a new correlation [5].

5 CONCLUSIONS

A recently developed method (eq. 2) to determine the primary particle diameter (or SSA) and number in agglomerates and aggregates by *in-situ* DMA-APM measurements during particle production is applied to ZrO_2 generated in a flame spray pyrolysis reactor. The model parameters (k_a & D_a) are based on multiparticle sintering simulations. The primary particle number and diameter of agglomerates and aggregates is calculated from mass-mobility measurements with known particle density without requiring separate microscopic or nitrogen adsorption measurements or fitting. Good agreement is found with primary particle diameters from BET measurements. The method works even for agglomerates or aggregates with d_m = 200 nm, thus indicating that the projected area is a good measure of agglomerate mobility if the primary particles are sufficiently small. Longer particle residence time at high temperatures and high concentrations resulted in larger primary particles. The fractal-like zirconia particles have a mass-mobility exponent, $D_{fm} \approx 2.15$, independent of investigated process conditions. These values are consistent with agglomerates formed by cluster-cluster coagulation or aggregates at the beginning of sintering.

REFERENCES

[1] J.H. Scheckman, P.H. McMurry, S.E. Pratsinis, Langmuir 25, 8248 - 8254, 2009.

[2] M.L. Eggersdorfer, D. Kadau, H.J. Herrmann, S.E. Pratsinis, Langmuir 27, 6358 - 6367, 2011.

[3] M.L. Eggersdorfer, S.E. Pratsinis, Aerosol Sci. Technol. 46, 347 - 353, 2012.

[4] S.N. Rogak, R.C. Flagan, Part. Part. Syst. Char. 9, 19 - 27, 1992.

[5] M.L. Eggersdorfer, D. Kadau, H.J. Herrmann, S.E. Pratsinis, J. Aerosol Sci. 46, 7-19, 2012.

[6] R. Botet, R. Jullien, M. Kolb, J. Phys. A 17, L75-L79, 1984.

[7] B. Buesser, A.J. Gröhn, S.E. Pratsinis, J. Phys. Chem. C 115, 11030-11035, 2011.

[8] L. Madler, H.K. Kammler, R. Mueller, S.E. Pratsinis, J. Aerosol Sci. 33, 369-389, 2002.

[9] P.H. McMurry, X. Wang, K. Park, K. Ehara, Aerosol Sci. Technol. 36, 227-238, 2002.

[10] M.J. Kirchhof, H.J. Schmid, W. Peukert, Phys. Rev. E 80, 026319, 2009.

[11] A.I. Medalia, J. Colloid Interface Sci. 24, 393-404, 1967.

[12] C.M. Sorensen, Aerosol Sci. Technol. 45, 755-769, 2011.